RSC Advances

PAPER

View Article Online
View Journal | View Issue

Cite this: *RSC Adv.*, 2024, **14**, 24942

Near-infrared-responsive Prussian blue nanocages loaded with 5-fluorouracil for combined chemotherapy and photothermal therapy in tumor treatment†

Zhongyi Guo, Kang Fu, Jingyi Sun, Wenhao Du, Qisheng Hao and Xiao Hu *

Received 24th June 2024
Accepted 5th August 2024

DOI: 10.1039/d4ra04609a

rsc.li/rsc-advances

Nanodrug delivery systems (NDDS) have been proposed to improve the targeting and bioavailability of chemotherapy drugs. The approach of drug loading *via* physical adsorption is facile to operate; however, there exists a risk of premature leakage. Coupling the drug molecules with the carrier through chemical reactions can guarantee the stability of the drug delivery process, yet the preparation procedure is relatively intricate. In this research, a kind of Prussian blue nanocage (PB Cage) was fabricated, and the phase change material, 1-pentadecanol, was used as the gating material to solidify 5-fluorouracil (5-FU) inside the nanocage. Upon irradiation with near-infrared (NIR) light, the temperature of the PB Cage can rise rapidly. When the temperature exceeds 43 °C, 1-pentadecanol undergoes a solid–liquid phase transition and subsequently releases 5-FU to inhibit DNA synthesis. Meanwhile, the photothermal therapy (PTT) mediated by the PB Cage is also capable of ablating tumor cells. The NDDS constructed based on PB has achieved the precise release of 5-FU triggered by NIR light, which may avoid side effects on normal tissues. Moreover, the combination of chemotherapy and photothermal therapy can efficaciously suppress the proliferation of tumor cells.

Introduction

Chemotherapy refers to the utilization of chemical drugs either systematically or locally in order to suppress the growth of tumors or directly eradicate tumors.[1,2] Notwithstanding that, there are certain inevitable side effects of chemotherapy, such as nausea, vomiting, hair loss, and bone marrow suppression, for tumor patients who have already metastasized or have no opportunity for surgery, chemotherapy is still regarded as a primary treatment plan to control the growth and metastasis of tumors to the greatest extent possible. Nanodrug delivery systems (NDDS) have been put forward to enhance the targeting and bioavailability of chemotherapy drugs within the body, while minimizing the damage to healthy tissues.[3,4] The combination of the drug and the carrier can be achieved through physical adsorption or covalent bond coupling.[5–7] Physical adsorption typically entails adsorbing drug molecules onto the surface or interior of nanocarriers, which is facile to operate, yet whether drugs will leak prematurely requires meticulous consideration. For example, the clinically chemotherapeutic drug mitoxantrone can be readily loaded into the micelles constructed by DSPE-PEG.[8] Coupling the drug molecules to the carrier *via* chemical reactions can guarantee stability in the drug delivery procedure, yet the preparation process is rather complex. Zhou *et al.* put forward a γ-glutamyl transpeptidase-responsive camptothecin–polymer conjugate which actively permeates throughout the tumor tissue by means of transcytosis. The conjugate demonstrated a strong antitumour activity in mouse models.[9]

Liposomes, polymers, and inorganic nanomaterials have all been investigated for the establishment of nanodrug delivery systems.[10,11] Metal–organic frameworks (MOFs) represent crystalline substances which are formed through the self-assembly of organic linkers and metal ions, possessing large specific areas and pore volumes.[12,13] In recent years, the application of MOFs in the biomedical domain has been progressively receiving attention, particularly in the areas of drug delivery, bioimaging, tissue engineering, and antibacterial.[14–17] The porosity and controllability of MOFs render them as ideal contenders for drug delivery. Through the embedding of drug molecules within the pores of MOFs-based NDDS, the controlled release and targeted delivery of drugs can be attained. Prussian blue (PB) is a type of MOFs with the formula $Fe_4[Fe(CN)_6]_3 \cdot nH_2O$. Nanoparticles fabricated using PB have adjustable morphology, excellent blood stability, biocompatibility, and biodegradability, and are capable of fulfilling the requirements of drug delivery.[18] By conducting charge transfer

Department of Hepatobiliary and Pancreatic Surgery, The Affiliated Hospital of Qingdao University, Qingdao, Shandong, 26000, PR China. E-mail: drhuxiao202@163.com

† Electronic supplementary information (ESI) available. See DOI: https://doi.org/10.1039/d4ra04609a

between Fe^{3+} and Fe^{2+} with cyanide ions, the Prussian blue nanoparticles (PB NPs) can convert near-infrared (NIR) light to thermal energy efficiently.[19,20] Therefore, the PB NPs have also been considered as a photothermal agent for photothermal therapy (PTT) of tumors. For instance, Liu *et al.* developed a versatile PB nanotheranostic platform loaded with therapeutic plasmid DNA (HSP70-p53-GFP) for NIR light-triggered thermos-controlled synergistic gene therapy/PTT.[21]

Phase change materials (PCMs) are materials that can undergo phase transition at exact temperatures and absorb or release a significant quantity of latent heat during the phase transition procedure.[22] Some studies have used PCMs as gated materials for drug controlled release. When the temperature reaches the phase change point, the PCM transforms from solid to liquid, thereby opening or closing the "gate" of drug release[23,24] In this manner, it is possible to achieve the precisely controlled release of drugs. It can release the appropriate dosage of drugs at a specific time and location as required, enhancing the curative effect of the drugs and minimizing side effects.

5-Fluorouracil (5-FU) is a typical chemotherapy drug in clinical settings for treating multiple types of solid tumors.[25] In this research, a kind of Prussian blue nanocage (PB Cage) was fabricated, and PCM, 1-pentadecanol, was used as the gating material to solidify 5-FU inside the nanocage (Fig. 1). PB Cage possesses excellent photothermal conversion capabilities. Upon irradiation by NIR light, the temperature of PB Cage can rise rapidly. When the temperature exceeds 43 °C, 1-pentadecanol undergoes a solid–liquid phase transition and subsequently releases 5-FU. Meanwhile, the PTT mediated by PB Cage is also capable of ablating tumor cells. The NDDS constructed based on PB has achieved the precise release of 5-FU triggered by NIR light, which may avoid side effects on normal tissues. Moreover, the combination of chemotherapy and photothermal therapy can efficaciously suppress the proliferation of tumor cells.

Results and discussion

Morphology and structure of nanocarriers

PB NPs are prepared through the hydrothermal method. $K_3[Fe(CN)_6]$ is taken as the precursor. In the acidic solution, the Fe^{3+} is slowly released and reduced to Fe^{2+}. The generated iron ions can immediately react with the precursor to generate PB NPs. This preparation approach is facile to operate and capable of obtaining nanoparticles with relatively high uniformity.[26] As shown in Fig. 2a, TEM images visually show that the PB NPs appear as solid cubes of uniform size with clear and complete boundaries. The hollow PB Cage can be obtained by etching the prepared PB NPs with HCl at high temperature. The edges

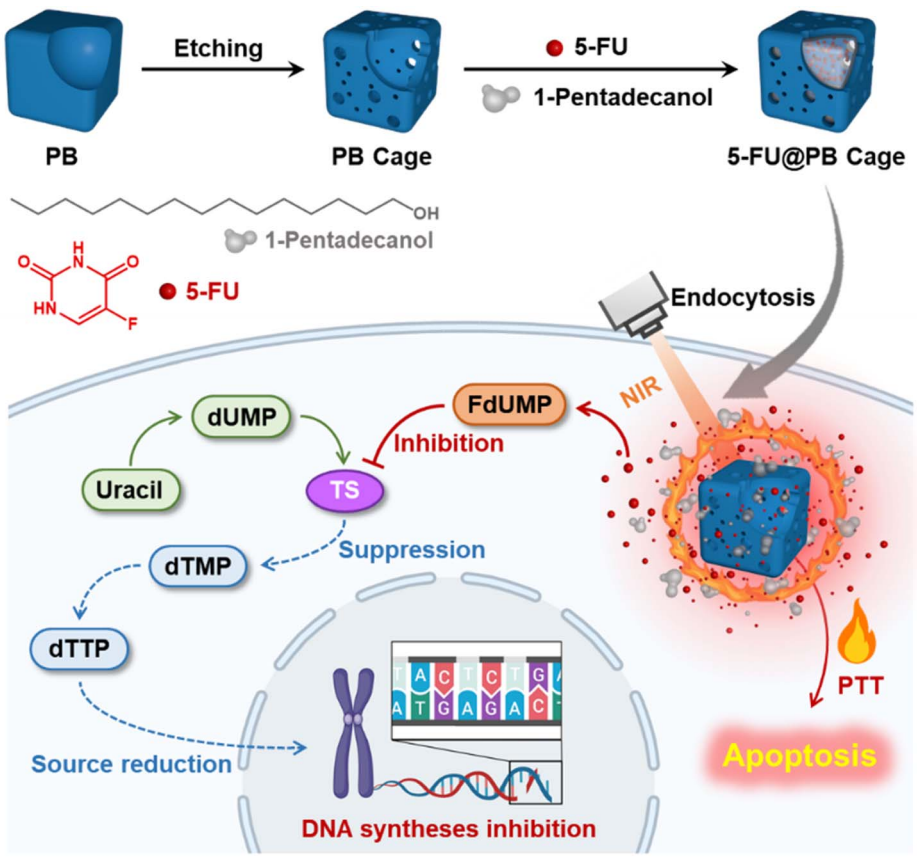

Fig. 1 The synthetic route of 5-FU@PB Cage and the schematic diagram of NIR-triggered increase in the temperature of 5-FU@PB Cage for achieving photothermal therapy and releasing 5-FU to inhibit DNA synthesis. Created in https://www.biorender.com.

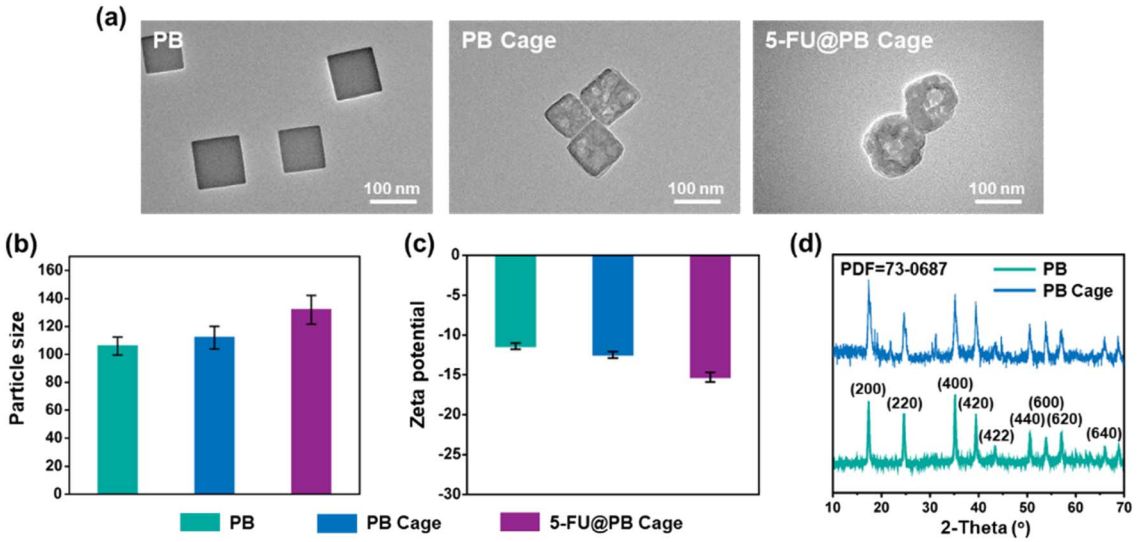

Fig. 2 The (a) TEM images, (b) particle size and (c) zeta potential of PB, PB Cage and 5-FU@PB Cage. (d) The XRD patterns of PB and PB Cage.

around the PB Cages were no longer sharp, and holes were visible on the surface of the PB Cage.

Fatty acids and fatty alcohols are phase change materials that are widely used in the field of biomedical materials.[27] Fatty acids can achieve stable solid–liquid phase change at a specific temperature, and the key parameters such as phase change temperature and phase change enthalpy can be precisely controlled by adjusting the types and compositions of fatty acids.[28] During the process of stirring the nanocage together with 1-pentadecanol and 5-FU, 1-pentadecanol and 5-FU enter the inner cavity through the holes on the surface of the nanocage. After the reaction, when the temperature was lowered below the phase transition temperature of PCM, the 1-pentadecanol transformed into a solid state and was fixed inside the nanocages. At this time, 5-FU was also solidified and stabilized inside the nanocages. Due to the solidification of the PCM inside and on the surface, the particle size of 5-FU@PB Cage is slightly larger than that of the nanocages, increasing from 110 nm to about 130 nm (Fig. 2a, b, S1 and S2†). Nanoparticles in the range of 100–200 nm have been shown to extravasate through vascular fenestrations of tumors (the enhanced permeation and retention effect (EPR effect)) and escape filtration by liver and spleen.[29] Consequently, this size range may be a trade-off between various factors. It can prevent rapid clearance by the kidneys, thereby enabling a relatively prolonged *in vivo* circulation time. Additionally, the interior has enough space to guarantee a considerable drug loading capacity (DLC). The particle size of the 5-FU@PB Cage remained stable when exposed to 50% fetal bovine serum (Fig. S3†). When the test lasted for 5 days, the particle size increased significantly. This might be due to the formation of protein crowns. However, the particle size was still below 200 nm and still within the appropriate range of the EPR effect.

These nanoparticles constructed based on PB show a negative electrical property (Fig. 2c). Nanoparticles with negatively charged surfaces can avoid non-specific adsorption, premature clearance by the immune system, and self-aggregation precipitation.[29,30] At the same time, this surface negatively charged characteristic also enables nanoparticles to reduce the formation of the protein corona, which is helpful to maintain the function and the long-term circulation of nanoparticles *in vivo*. The XRD pattern of both PB NPs and PB Cages exhibited a single crystal structure corresponding to PB (Powder Diffraction File no. 73-0687, Joint Committee on Powder Diffraction Standards), signifying that the crystal phase of PB Cage was still maintained after the etching process (Fig. 2d).

The FTIR spectrum (Fig. 3a) of 5-FU@PB Cage shows that the absorption peaks appearing at 1610 cm^{-1} and 2100 cm^{-1} are ascribed to the stretching vibration peaks of –COO– in PB and –CN in Fe^{2+}-CN-Fe^{3+}. The characteristic absorption peaks at 2915 cm^{-1} and 1657 cm^{-1} are attributed to 1-pentadecanol and 5-FU. PB Cage exhibits a wide UV-vis absorption band with an absorption peak approximately at 715 nm. Whereas 5-FU@PB Cage simultaneously has the characteristic peak of PB Cage and also has the strong absorption corresponding to 5-FU at 265 nm and the absorption corresponding to 1-pentadecanol at the range of 200–220 nm (Fig. 3b). These results confirm that 5-FU was solidified in 1-pentadecanol and encapsulated inside the PB Cage. Elements samples were detected by X-ray photoelectron spectroscopy (XPS, Fig. 3c). The C, N, and Fe elements of the PB Cage were presented in the wide-scan XPS spectra, while extra F element (693 eV) from the 5-FU was detected in the 5-FU@PB Cage. The DLC of 5-FU in the 5-FU@PB Cage is about 9.6 wt%. In addition, the drug loading efficacy of nanocarriers without adding 1-pentadecanol is about 10.3 wt%. This indicates that the addition of 1-pentadecanol does not influence the loading of the drug.

Photothermal conversion and controlled release

The penetration of NIR light to biological tissues can reach the millimeter or even centimeter level, enabling the detection and treatment of deep tissues.[31] The molar absorptivity of PB NPs at

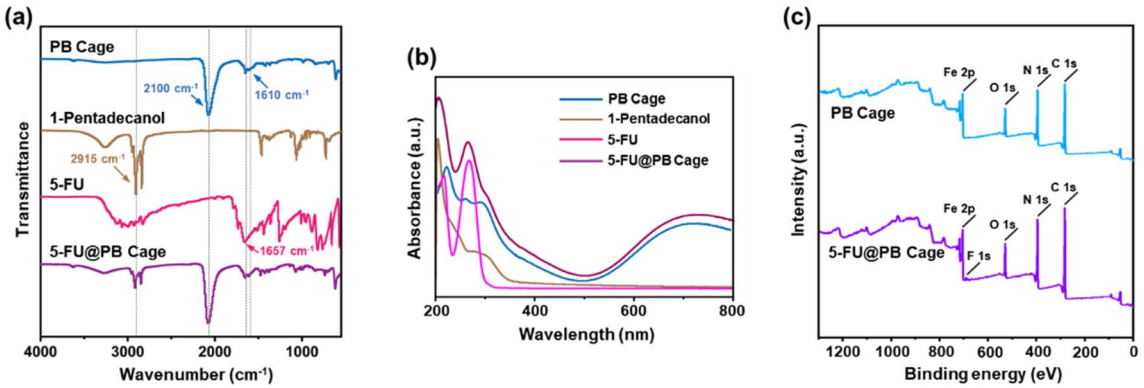

Fig. 3 (a) FTIR spectra and (b) UV absorption curves of PB Cage, 1-pentadecanol, 5-FU and 5-FU@PB Cage. (c) XPS wide-scan spectrum of PB Cage and 5-FU@PB Cage.

808 nm is significantly higher than that of conventional photothermal agents, providing strong assistance for efficient photothermal conversion.[32] enabling the detection and treatment of deep tissues. Different concentrations of 5-FU@PB Cage solutions (25, 50, 100 μg mL^{-1}) and PBS solutions were irradiated by NIR light (1.0 W cm^{-2}, 808 nm), and temperature changes were recorded. The PBS solution remained approximately at room temperature throughout the testing period, and there was no increase in the temperature. While the temperature of the 5-FU@PB Cage solution increased significantly and showed a concentration-dependent manner. When the concentration reached 50 μg mL^{-1}, it was detected that the temperature rose rapidly to about 40 °C in the first 2 min, and could finally reach about 48 °C (Fig. 4a). The phase transition temperature of 1-pentadecanol is 43 °C. So, when NIR light irradiates the 5-FU@PB Cage for approximately 3 min, 5-FU may be released along with the solid–liquid transition of 1-pentadecanol. Meanwhile, the appropriate temperature range for photothermal therapy is 45–60 °C. This implies that the prepared 5-FU@PB Cage fulfills the requirements of photothermal therapy. Fig. 4b shows the temperature change visually presented by a thermal imager. After five cycles of irradiation by NIR light, the peak temperature did not decrease, indicating that the photothermal conversion of 5-FU@PB Cage is stable (Fig. 4c). This implies that the prepared 5-FU@PB Cage fulfills the requirements of photothermal therapy. Stable photothermal conversion can ensure the continuous generation of sufficient and constant heat during multiple treatment processes, thereby ensuring sustained and effective killing of the tumor, and enhancing the repeatability of the treatment effect. It helps to maintain the accuracy of treatment, reduces the fluctuation or uncertainty risk of the treatment effect caused by unstable photothermal conversion, and enables photothermal therapy to play a better role in practical applications.

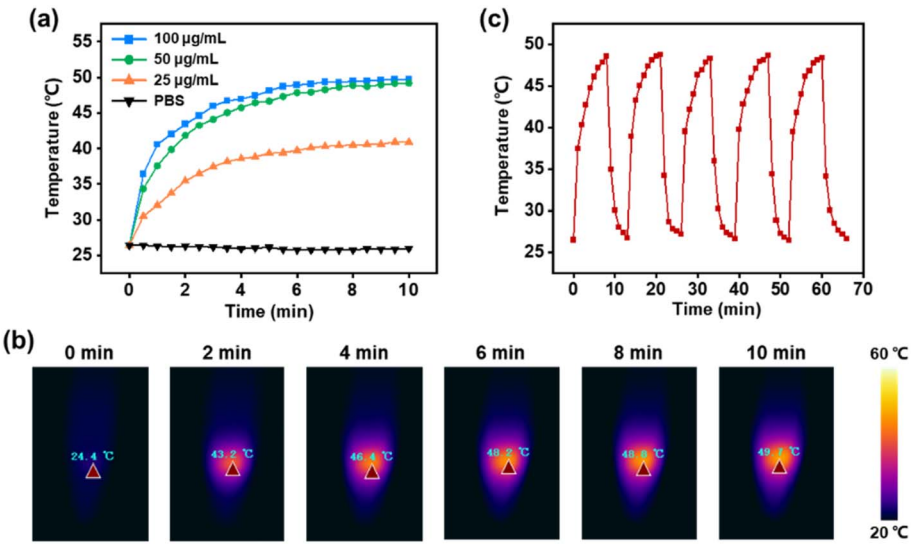

Fig. 4 (a) The temperature variation of 5-FU@PB Cage solution upon exposure to NIR light. (b) Real-time thermal imagings of 5-FU@PB Cage solution with 808 nm laser irradiation for the predetermined time. (c) The photothermal stability of 5-FU@PB Cage after 5 repeated exposures to NIR light.

Under continuous NIR light, the release process of 5-FU (Fig. 5a) was observed to be consistent with the temperature rise trend of the 5-FU@PB Cage. Especially in the first 10 min, 5-FU was released rapidly due to the melting of 1-pentadecanol. Without NIR light, the release of 5-FU can hardly be detected. Cyclic controlled release triggered by NIR light was then tested. It was found that upon the deactivation of the NIR light, the release of 5-FU stopped accordingly, and the release was detected again when the solution was exposed to NIR light (Fig. 5b). Note that this "on–off" release is more pronounced in the first two cycles. The subsequent cycles might be attributed to an insufficient amount of phase change material within the cage, and even when it is in the "off" state, it is no longer capable of effectively restraining the drug molecules. This kind of near-infrared-triggered drug release is beneficial for avoiding drug leakage in non-targeted regions, thereby reducing the toxic and side effects on normal tissues.

Blood compatibility of nanocarriers

Good blood compatibility allows nanocarriers to stay stable during the circulation process, avoiding coagulation and thrombosis, and ensuring the precise delivery of drugs to the target site.[33] RBCs dispersed in Triton X-100 were regarded as positive control group, and the hemolysis rate of the carrier was quantitatively analyzed by detecting the absorbance of the supernatant. As shown in Fig. 6a, the hemolysis rate of 5-FU@PB Cage at all concentrations is less than 1%. Similar to the negative control group (PBS), the supernatants of all 5-FU@PB Cage groups are transparent, while the positive control group (Triton X-100) appears red due to the rupture of RBCs (Fig. 6b). It can be observed by using an inverted fluorescence microscope that the RBCs co-incubated with 5-FU@PB Cage still present a biconcave disc shape, while the morphology of the RBCs treated with Triton X-100 appears fragmented (Fig. 6c). The results demonstrate that 5-FU@PB Cage possesses good blood compatibility.

Cellular internalization of nanocarriers

The cell membrane acts as a barrier during the process of drug delivery. The effective internalization of nanocarriers is crucial for the enrichment of drugs within cells. The internalization of PB Cage by HepG2 cells was detected by flow cytometry. The Nile red was solidified together with 1-pentadecanol inside the PB Cage. The efficiency of cellular uptake was determined by measuring the fluorescence intensity emitted by the positive cells. After the cells were incubated with the sample for 4 h, the internalization rate of PB Cage was 77.9% (Fig. 7a). To visualize the internalization of the carrier, FITC (green) was employed to label the PB Cage and Hoechst (blue) to label the nucleus. Obvious green fluorescence was observed using CLMS in HepG2 cells 4 h after PB Cage treatment (Fig. 7b).

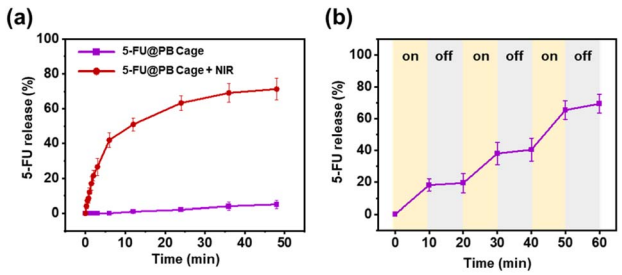

Fig. 5 5-FU release profiles of 5-FU@PB Cage under (a) continuous NIR light and (b) alternating NIR light.

Antitumor performance of nanocarriers

HepG2 cells are tumor cells extracted from the liver tissue of a patient with hepatocellular carcinoma, which grows rapidly and retains some of the metabolic activities of liver cells. 5-FU is commonly used in clinical practice to treat liver cancer, and it can exert an antitumor effect by interfering with the nucleic acid synthesis of cancer cells. L929 cells, serving as the control group, are mouse fibroblast cells that possess excellent proliferative capacity and stability. The photothermal therapeutic effect of PB Cage and the curative effect of combined treatment with 5-FU were evaluated *in vitro* (Fig. 8a and S4†). In the absence of NIR irradiation, both types of cells treated with PB Cage and 5-FU@PB Cage exhibited a high survival rate (greater than 80%) even at high concentrations. This suggests that PB Cage and 5-FU@PB Cage possess excellent biocompatibility. This is a predictable result, as PB is already a clinical drug approved by the US Food and Drug Administration (FDA). On the other hand, it also indicates that 5-FU can be stably solidified inside 5-FU@PB Cage and will not release 5-FU without being activated by NIR light. The controlled release triggered by NIR light can effectively avoid the side effects of chemotherapy drugs on normal tissues in clinical application. Correspondingly, after a period of NIR irradiation, the cell survival rate in all tested concentration ranges has decreased significantly, especially when the concentration was higher than 150 μg mL^{-1}.

Upon being irradiated by NIR light, the temperature of the nanocage rose rapidly, and the cells died due to high temperature. Upon reaching the phase transition temperature of 1-pentadecanol, 5-FU will be released from the nanocage along with liquid 1-pentadecanol. Subsequently, 5-FU will be transformed into 5-fluoro-2′-deoxyuridine-5′-monophosphate (FdUMP) within the cells.[34] As illustrated in Fig. 1, FdUMP is capable of inhibiting the activity of thymidylate synthase (TS), thereby preventing 2′-deoxyuridylate (dUMP) from being converted into deoxythymidylate (dTMP), interfering with the synthesis of DNA, and consequently exerting a role in restraining the growth of tumor cells. As a result, lower cell survival rates were recorded with the combination of chemotherapy and photothermal therapy.

The live/dead staining assay visually presents the survival status of cells after treatment with 5-FU@PB Cage (150 μg mL^{-1}) with or without NIR light (Fig. 8b). Firstly, the cells were treated with 5-FU@PB Cage for 4 h to internalize the nanocarriers. Subsequently, a group of cells were irradiated with NIR light for 10 min to trigger the release of 5-FU and photothermal therapy. In the group without NIR irradiation, the cells presented

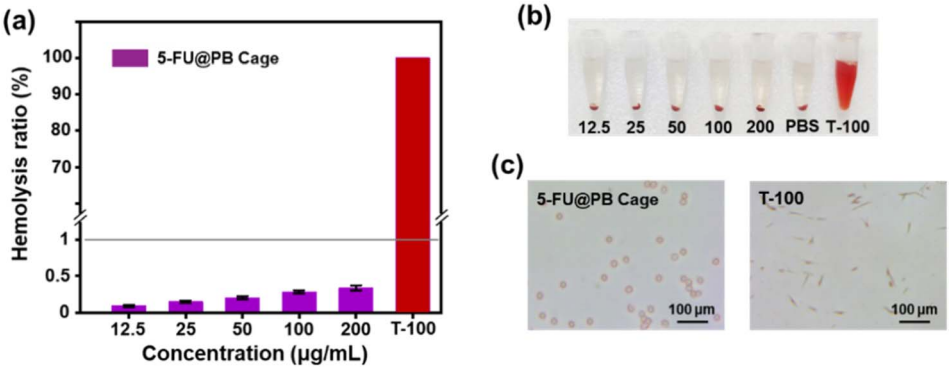

Fig. 6 (a) Hemolysis rate of 5-FU@PB Cage. (b) Hemolysis assessment of 5-FU@PB Cage, unit: mg mL^{-1}. (c) Inverted fluorescence images of red blood cells treated with 5-FU@PB Cage and Triton X-100, respectively.

a favorable survival status (green fluorescence), and only a few apoptotic cells were observed (red fluorescence). In the NIR irradiation group, the green fluorescence exhibited a significant decrease while the red fluorescence showed an increase. This trend is in line with the outcomes of the cell survival rate.

Experimental

Materials

Polyvinylpyrrolidone (PVP), 1-pentadecanol, and potassium ferricyanide ($K_3[Fe(CN)_6]$) were obtained from Maclin Biochemical Technology Co., Ltd (China). 3-(4,5-Dimethyl-2-thiazolyl)-2,5-diphenyltetrazolium bromide (MTT), Triton X-100, and 5-fluorouracil (5-FU) were obtained from Aladdin Reagent Co., Ltd (China). Hydrochloric acid (HCl), dimethyl sulfoxide (DMSO) and methanol were procured from Sinopharm Chemical Reagent Co., Ltd (China). Fetal bovine serum (FBS), Dulbecco's Modified Eagle's Medium (DMEM), penicillin-streptomycin, and trypsin were procured from Gibco Life Technologies (Carlsbad, CA, USA).

Preparation of PB nanoparticles

The preparation of PB NPs referred to reported methods.[18] First, 6 g of PVP was dissolved in 80 mL of HCl solution (0.01 mol mL^{-1}). The solution was stirred until transparent at room temperature. Then 30 g of $K_3[Fe(CN)_6]$ was added to the solution, and a clarified orange solution was obtained after 20 min of ultrasonic treatment. After the reaction at room temperature for 30 min, the reactants were placed in an oil bath at 80 °C for 20 h. The precipitation was collected by centrifugation (10 min,

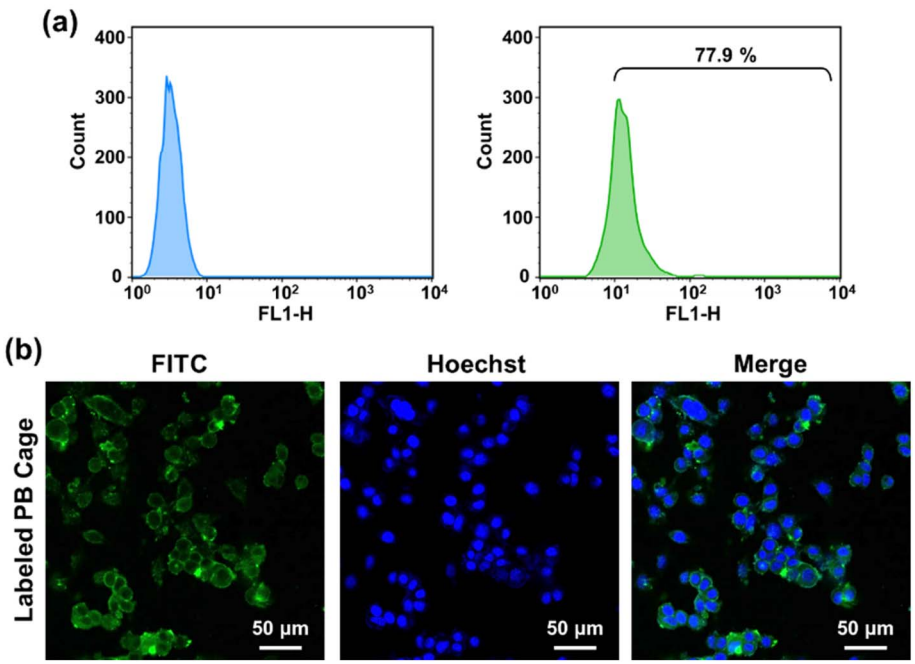

Fig. 7 (a) Flow cytometry of HepG2 cells incubated with the PB Cage loaded with Nile red. (b) Representative fluorescence images of HepG2 cells incubated with PB Cage loaded with FITC.

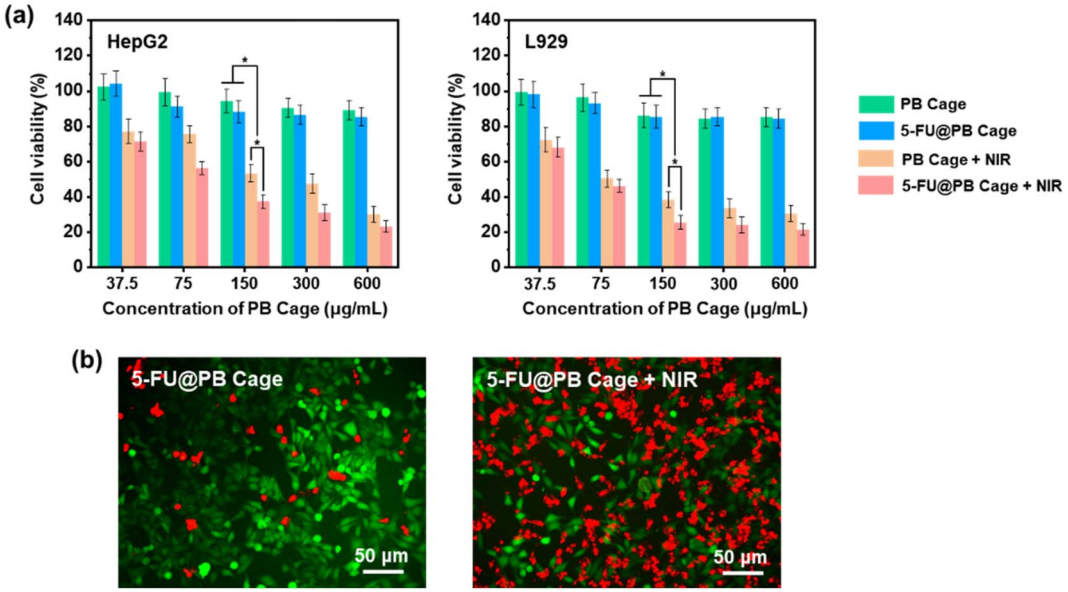

Fig. 8 (a) Cell viability of the HepG2 and L929 cells served with different concentrations of PB Cage and 5-FU@PB Cage with or without NIR irradiation (mean ± SD, $n = 6$, $^*p < 0.05$). (b) Double-staining of HepG2 cells subjected to 5-FU@PB Cage with or without NIR irradiation.

10 000 rpm) and washed three times with deionized water. PB NPs were obtained after vacuum drying.

Preparation of PB cages

100 mg of PB and 500 mg of PVP were added to 100 mL of HCl solution (1 mol L^{-1}), and the solution was vigorously stirred until PB and PVP were completely dispersed. After stirring at room temperature for 3 h, the solution was transferred to the autoclave and continued to react at 140 °C for 4 h. After waiting for the autoclave to cool to room temperature, centrifuge the reaction solution (10 min, 10 000 rpm) and collect the precipitate. Wash the precipitate with deionized water three times and then vacuum dry to obtain the PB Cage.

Encapsulation of drugs

5 mg of 1-pentadecanol was dissolved in 2 mL of methanol. 1 mg of PB Cage and 4 mg of 5-FU were dispersed into 1 mL of deionized water and the suspension was added to the aforementioned 1-pentadecanol solution. The mixture was vigorously stirred at ambient temperature for 4 h. The precipitation was gathered through centrifugation (10 min, 9000 rpm, 4 °C) after the reaction. Subsequently, the precipitate was delicately washed with methanol and subjected to vacuum drying in order to acquire 5-FU loaded nanocarriers (5-FU@PB Cage).

Characterization

The samples were dispersed in deionized water and dripped onto the grids with lacey carbon support film. Upon the samples being dried, the morphology of the samples was observed by a transmission electron microscope (TEM, JEM-2100Plus, JEOL). The particle size and zeta potential of nanoparticles were determined through a laser particle size and potential analyzer (Zetasizer Nano-ZS90, Malvern Instruments Ltd). The test was repeated three times for each sample. The phase analysis and crystalline structure testing of were conducted by an X-ray diffractometer (XRD, Rigaku MiniFlex 600) with a graphite monochromator using Cu Kα radiation ($\lambda = 1.54056$ Å), operating at 40 kV and 15 mA. The composition was analyzed by Fourier transform infrared (FTIR) spectra (Nicolet 6700, Thermo Scientific), XPS analysis was employed to determine the elemental composition (Axis Supra+, JPN), and UV-visible spectra (UH4150, Hitachi High-Technologies).

Evaluation of the photothermal conversion performance

The sample was gradient diluted and 0.5 mL of the sample was irradiated with NIR light (808 nm, 1.0 W cm^{-2}). Temperature was recorded at intervals of 60 s. At the same time, the temperature change of the solution was recorded by a thermal imager. During the photothermal stability test, the solution was subjected to irradiation with NIR light (808 nm, 1.0 W cm^{-2}) until the temperature was stable, then the light source is deactivated until the solution has cooled down to room temperature. Turn on the NIR light to irradiate the sample again, and repeat the NIR irradiation cycle while recording the temperature changes.

Drug release

5-FU@PB Cage suspension was placed in an eppendorf tube. The sample was subjected to NIR light (808 nm, 1.0 W cm^{-2}) and 4 μL suspension was removed at a predetermined time to measure absorbance (at 265 nm) by a UV-visible spectrophotometer. For detecting the cyclic drug release performance of the nanocarriers, the solution was irradiated with NIR light (808 nm, 1.0 W cm^{-2}) every 10 min for 10 min. The 5-FU@PB Cage suspension was centrifuged and 4 μL of supernatant was

taken to measure the absorbance (at 265 nm) before and after each NIR irradiation by a UV-visible spectrophotomete. The calculation of DLC refers to the previous study.[35]

Blood compatibility test

Fresh blood from tail vein of mice was collected, centrifuged and washed with sterilized normal saline to obtain red blood cells (RBCs). 500 μL of RBCs suspension (in PBS) was respectively mixed with 500 μL of 5-FU@PB Cage suspension with a series of concentration gradients, Triton X-100 (positive control group), and PBS (negative control group). Upon incubation at 37 °C for 1 h, the supernatant was gathered through centrifugation (10 min, 3000 rpm). Then supernatants were placed in a 96-well plate and the absorbance at 570 nm was measured through a Varison Flash reader. The hemolysis rate was calculated according to the formula: Hemolysis (%) = $[(A_t - A_n)/(A_p - A_n)] \times 100\%$. A_t represents the absorbance value of the sample, A_p and A_n represent the absorbance values of the positive and negative groups, respectively. Three parallel experiments were conducted on each group. The morphology of RBCs that treated with 5-FU@PB Cage solution (200 mg mL^{-1}) or Triton X-100 was captured by an inverted fluorescence microscope.

Cellular internalization

FITC was encapsulated in the PB Cage for imaging of nanoparticles in cells. HepG2 cells were inoculated into confocal culture dishes (1×10^5 cells per mL) and cultured under standard condition for 24 h. Subsequently, the culture medium was substituted with fresh medium containing FITC@PB Cage. After 4 h of culture, the cells were marked by Hoechst for 10 min. The cells of the experimental group were then irradiated with NIR light for a period of 5 min (808 nm, 1.0 W cm^{-2}). The cells were then gently washed 3 times with PBS and fixed with 4% paraformaldehyde solution. The fluorescence of the cells was detected by means of a laser confocal microscopy (CLSM, Axio-Imager LSM-800, Zeiss). Nile red, as the fluorescent probe, was encapsulated in the PB Cage for flow cytometry. HepG2 cells were inoculated into 6-well plates (1×10^6 cells per mL) and cultured for 24 h. The PB Cage was then added and the culture continued for 4 h. After reaching the predetermined time, the cells were washed with PBS followed by digestion. Cells were gathered and re-suspended in 500 μL of PBS for flow cytometry (FACS Calibur, BD).

Evaluation of the cytotoxicity *in vitro*

The HepG2 cell line and L929 cell line were selected for MTT assay. Two types of cells were inoculated into 96-well plates (1×10^4 cells per well) and cultured for 24 h. HepG2 cells were cultured in DMEM medium, whereas L929 cells were cultured in RPMI 1640 medium. Varying concentrations of PB Cage and 5-FU@PB Cage were dispersed in the medium to replace the old culture medium. Some of the wells were subsequently irradiated with NIR light (808 nm, 1.0 W cm^{-2}). Upon the continuation of the culture for 24 h, the medium was eliminated and 100 μL of MTT solution (0.5 mg mL^{-1} in PBS) was added to each well. After 4 h, the MTT solution within the well was eliminated and 100 μL of DMSO was introduced. The absorbance (OD 490 nm) of the solution within each well was gauged by means of a microplate reader (SpectraMax M3). The cell viability was computed in accordance with the formula: Cell viability (%) = $OD_{sample}/OD_{control} \times 100\%$. OD_{sample} represents the absorbance value of cells that have been treated with samples, while $OD_{control}$ indicates the absorbance value of cells cultured in the normal medium.

In the live/dead staining assay, HepG2 cells were inoculated into 12-well plates (5×10^4 cells per well) and incubated for 24 h. The former medium was subsequently substituted with a medium containing 5-FU@PB Cage (150 μg mL^{-1}). After 4 h, some wells were irradiated with NIR light (808 nm, 1.0 W cm^{-2}) for 10 min. After further cultivation for 20 h, the cells were stained according to the steps of the live/dead cell double-staining kit. The cells were observed and imaged using a fluorescence microscope.

Statistical analysis

All experiments were repeated more than 3 times. Comparison analysis between groups was conducted by *t*-test ($*p < 0.05$). Data were taken as mean ± standard error.

Conclusions

A certain type of PB-based nanocage possessing photothermal conversion effect was fabricated. The phase change material 1-pentadecanol was used as a gating material to solidified the typical clinical chemotherapy drug 5-FU inside the PB Cage. The constructed nanocarrier exhibits good biocompatibility and an ideal drug loading capacity. Only upon being triggered by NIR light, 5-FU will be discharged from the nanocage along with the solid–liquid phase change of 1-pentadecanol. In this manner, the leakage of chemotherapy drugs during the *in vivo* circulation and the uncontrollable release at non-targeted sites are avoided. Undesirable side effects are also reduced. Furthermore, the increase in the temperature of the PB Cage will also exert the effect of photothermal therapy. The prepared nanocarrier combines chemotherapy and photothermal therapy to achieve multiple effects, including synergistic enhancement, accurately killing tumor cells, and reducing side effects.

Data availability

Data for this article are available at Weiyun Cloud at **https://share.weiyun.com/47I4WHJ8**.

Author contributions

Zhongyi Guo: conceptualization, formal analysis, data curation, and writing – original draft; Kang Fu: formal analysis, investigation, and data curation; Jingyi Sun: validation, data curation, and visualization; Wenhao Du and Qisheng Hao: validation; Xiao Hu: conceptualization, supervision, funding acquisition, and project administration.

Conflicts of interest

There are no conflicts to declare.

Acknowledgements

This work was supported by the National Natural Science Foundation of China (52075277).

Notes and references

1 A. E. Pomeroy, E. V. Schmidt, P. K. Sorger and A. C. Palmer, Drug independence and the curability of cancer by combination chemotherapy, *Trends Cancer*, 2022, **8**, 915–929.

2 Brianna and S. H. Lee, Chemotherapy: how to reduce its adverse effects while maintaining the potency?, *Med. Oncol.*, 2023, **40**, 88.

3 C. Y. Zhao, R. Cheng, Z. Yang and Z. M. Tian, Nanotechnology for cancer therapy based on chemotherapy, *Molecules*, 2018, **23**, 826.

4 W. C. Wu, Y. Y. Pu and J. L. Shi, Nanomedicine-enabled chemotherapy-based synergetic cancer treatments, *J. Nanobiotechnol.*, 2022, **20**, 4.

5 M. M. Yan, S. Wu, Y. H. Wang, M. H. Liang, M. B. Wang, W. T. Hu, G. C. Yu, Z. W. Mao, F. H. Huang and J. Zhou, Recent progress of supramolecular chemotherapy based on host–guest interactions, *Adv. Mater.*, 2024, **36**, 2304249.

6 Q. Wang, N. Jiang, B. Fu, F. Huang and J. F. Liu, Self-assembling peptide-based nanodrug delivery systems, *Biomater. Sci.*, 2019, **7**, 4888–4911.

7 Y. Sun, Q. M. Wu, Q. Y. Fu, H. L. Cong, Y. Q. Shen, B. Yu and H. Hu, Reactive oxygen species-responsive polyprodrug micelles deliver cell cycle regulators for chemosensitization, *Talanta*, 2024, **267**, 125242.

8 Z. Q. Chen, S. F. Li, F. Z. Li, C. Qin, X. L. Li, G. C. Qing, J. J. Wang, B. Z. Xia, F. X. Zhang, L. L. Meng, X. J. Liang and Y. Y. Xiao, DNA damage inducer mitoxantrone amplifies synergistic mild-photothermal chemotherapy for TNBC *via* decreasing heat shock protein 70 expression, *Adv. Sci.*, 2023, **10**, 2206707.

9 Q. Zhou, S. Q. Shao, J. Q. Wang, C. H. Xu, J. J. Xiang, Y. Piao, Z. X. Zhou, Q. S. Yu, J. B. Tang, X. R. Liu, Z. H. Gan, R. Mo, Z. Gu and Y. Q. Shen, Enzyme-activatable polymer-drug conjugate augments tumour penetration and treatment efficacy, *Nat. Nanotechnol.*, 2019, **14**, 799–809.

10 Z. S. Guo, J. H. Ye, X. H. Cheng, T. S. Wang, Y. Zhang, K. L. Yang, S. Y. Du and P. Y. Li, Nanodrug delivery systems in antitumor immunotherapy, *Biomater. Res.*, 2024, **28**, 0015.

11 Q. M. Wu, Y. Hu, B. Yu, H. Hu and F. J. Xu, Polysaccharide-based tumor microenvironment-responsive drug delivery systems for cancer therapy, *J. Controlled Release*, 2023, **362**, 19–43.

12 Z. X. Lin, J. J. Richardson, J. J. Zhou and F. Caruso, Direct synthesis of amorphous coordination polymers and metal–organic frameworks, *Nat. Rev. Chem.*, 2023, **7**, 273–286.

13 J. Fonseca, L. X. Meng, I. Imaz and D. Maspoch, Self-assembly of colloidal metal–organic framework (MOF) particles, *Chem. Soc. Rev.*, 2023, **52**, 2528–2543.

14 J. Yang, D. H. Dai, X. Zhang, L. S. Teng, L. J. Ma and Y. W. Yang, Multifunctional metal–organic framework (MOF)-based nanoplatforms for cancer therapy: from single to combination therapy, *Theranostics*, 2023, **13**, 295–323.

15 C. Q. Shu, C. Qin, L. Chen, Y. F. Wang, Z. Shi, J. M. Yu, J. M. Huang, C. Q. Zhao, Z. G. Huan, C. T. Wu, M. Zhu and Y. F. Zhu, Metal–organic framework functionalized bioceramic scaffolds with antioxidative activity for enhanced osteochondral regeneration, *Adv. Sci.*, 2023, **10**, 2206875.

16 D. W. Luo, J. F. Huang, Y. H. Jian, A. Singh, A. Kumar, J. Q. Liu, Y. Pan and Q. Ouyang, Metal–organic frameworks (MOFs) as apt luminescent probes for the detection of biochemical analytes, *J. Mater. Chem. B*, 2023, **11**, 6802–6822.

17 W. J. Xie, J. Y. Chen, X. T. Cheng, H. Feng, X. Zhang, Z. Zhu, S. S. Dong, Q. B. Wan, X. B. Pei and J. Wang, Multi-mechanism antibacterial strategies enabled by synergistic activity of metal–organic framework-based nanosystem for infected tissue regeneration, *Small*, 2023, **19**, 2205941.

18 Y. Liu, B. J. Yue, R. R. Wang, H. L. Cong, H. Hu, B. Yu and Y. Q. Shen, Photothermal-responsive Prussian blue nanocages loaded with thrombin for tumor starvation therapy and photothermal therapy, *Biomater. Sci.*, 2023, **11**, 4938–4947.

19 H. A. Hoffman, L. Chakrabarti, M. F. Dumont, A. D. Sandler and R. Fernandes, Prussian blue nanoparticles for laser-induced photothermal therapy of tumors, *RSC Adv.*, 2014, **4**, 29729–29734.

20 L. C. Wang, P. Y. Chiou, Y. P. Hsu, C. L. Lee, C. H. Hung, Y. H. Wu, W. J. Wang, G. L. Hsieh, Y. C. Chen, L. C. Chang, W. P. Su, D. Manoharan, M. C. Liao, S. Thangudu, W. P. Li, C. H. Su, H. K. Tian and C. S. Yeh, Prussian blue analog with separated active sites to catalyze water driven enhanced catalytic treatments, *Nat. Commun.*, 2023, **14**, 4709.

21 Y. J. Liu, G. M. Shu, X. Li, H. B. Chen, B. Zhang, H. Z. Pan, T. Li, X. Q. Gong, H. J. Wang, X. L. Wu, Y. Dou and J. Chang, Human HSP70 promoter-based Prussian blue nanotheranostics for thermo-controlled gene therapy and synergistic photothermal ablation, *Adv. Funct. Mater.*, 2018, **28**, 1802026.

22 J. Giro-Paloma, M. Martínez, L. F. Cabeza and A. I. Fernández, Types, methods, techniques, and applications for microencapsulated phase change materials (MPCM): a review, *Renew. Sustainable Energy Rev.*, 2016, **53**, 1059–1075.

23 C. L. Zhu, D. Huo, Q. S. Chen, J. J. Xue, S. Shen and Y. N. Xia, A eutectic mixture of natural fatty acids can serve as the gating material for near-infrared-triggered drug release, *Adv. Mater.*, 2017, **29**, 1703702.

24 J. H. Li, M. X. Yang, X. J. Sun, X. Yang, J. J. Xue, C. L. Zhu, H. Liu and Y. N. Xia, Micropatterning of the ferroelectric phase in a poly(vinylidene difluoride) film by plasmonic

heating with gold nanocages, *Angew. Chem., Int. Ed.*, 2016, **55**, 13828–13832.
25 A. Mafi, M. Rezaee, N. Hedayati, S. D. Hogan, R. J. Reiter, M. H. Aarabi and Z. Asemi, Melatonin and 5-fluorouracil combination chemotherapy: opportunities and efficacy in cancer therapy, *Cell Commun. Signal.*, 2023, **21**, 33.
26 B. Kong, J. Tang, Z. X. Wu, J. Wei, H. Wu, Y. C. Wang, G. F. Zheng and D. Y. Zhao, Ultralight mesoporous magnetic frameworks by interfacial assembly of Prussian blue nanocubes, *Angew. Chem., Int. Ed.*, 2014, **53**, 2888–2892.
27 S. Kahwaji and M. A. White, Organic phase change materials for thermal energy storage: influence of molecular structure on properties, *Molecules*, 2021, **26**, 6635.
28 J. C. Qiu, D. Huo and Y. N. Xia, Phase-change materials for controlled release and related applications, *Adv. Mater.*, 2020, **32**, 2000660.
29 E. Blanco, H. Shen and M. Ferrari, Principles of nanoparticle design for overcoming biological barriers to drug delivery, *Nat. Biotechnol.*, 2015, **33**, 941–951.
30 K. Abstiens, S. M. Figueroa, M. Gregoritza and A. M. Goepferich, *Soft Matter*, 2019, **15**, 709–720.
31 Y. Chen, S. Wang and F. Zhang, Near-infrared luminescence high-contrast *in vivo* biomedical imaging, *Nat. Rev. Bioeng.*, 2023, **1**, 60–78.
32 W. Gao, Y. Wang, Y. Y. Zheng and X. J. Cai, Prussian blue nanoparticle: from a photothermal conversion agent and a drug delivery system, to a bioactive drug, *Acc. Mater. Res.*, 2024, **5**, 687–698.
33 S. Q. Guo, Y. A. Shi, Y. Z. Liang, L. Z. Liu, K. X. Sun and Y. X. Li, Relationship and improvement strategies between drug nanocarrier characteristics and hemocompatibility: what can we learn from the literature, *Asian J. Pharm. Sci.*, 2021, **16**, 551–576.
34 S. Vodenkova, T. Buchler, K. Cervena, V. Veskrnova, P. Vodicka and V. Vymetalkova, 5-Fluorouracil and other fluoropyrimidines in colorectal cancer: past, present and future, *Pharmacol. Ther.*, 2020, **206**, 107447.
35 J. F. Chen, F. F. Xue, W. X. Du, H. Z. Yu, Z. B. Yang, Q. J. Du and H. R. Chen, An endogenous H_2S-activated nanoplatform for triple synergistic therapy of colorectal cancer, *Nano Lett.*, 2022, **22**, 6156–6165.